

# Hierarchical Spatial Proximity Reasoning for Vision-and-Language Navigation

Ming Xu<sup>†</sup>, Zilong Xie<sup>†</sup>

<sup>†</sup>Liaoning Technical University, Liaoning, China

<https://github.com/18979705623/HSPR>

## Abstract

Most Vision-and-Language Navigation (VLN) algorithms tend to make decision errors, primarily due to a lack of visual common sense and insufficient reasoning capabilities. To address this issue, this paper proposes a Hierarchical Spatial Proximity Reasoning (HSPR) model. Firstly, we design a Scene Understanding Auxiliary Task (SUAT) to assist the agent in constructing a knowledge base of hierarchical spatial proximity for reasoning navigation. Specifically, this task utilizes panoramic views and object features to identify regions in the navigation environment and uncover the adjacency relationships between regions, objects, and region-object pairs. Secondly, we dynamically construct a semantic topological map through agent-environment interactions and propose a Multi-step Reasoning Navigation Algorithm (MRNA) based on the map. This algorithm continuously plans various feasible paths from one region to another, utilizing the constructed proximity knowledge base, enabling more efficient exploration. Additionally, we introduce a Proximity Adaptive Attention Module (PAAM) and Residual Fusion Method (RFM) to enable the model to obtain more accurate navigation decision confidence. Finally, we conduct experiments on publicly available datasets including REVERIE, SOON, R2R, and R4R to validate the effectiveness of the proposed approach.

## 1. Introduction

In recent years, Vision-and-Language Navigation (VLN) [1] tasks in Embodied AI have demonstrated significant value in areas such as social services, rescue operations, and human-computer interaction. VLN aims to enable agents to understand human instructions, recognize visual observations in the real world, and achieve precise navigation in unseen environments. Based on the language instructions, VLN can be divided into fine-grained navigation that provides step-by-step instructions (e.g., R2R [1]), goal-oriented coarse-grained navigation (e.g., REVERIE [2]), and dialogue-based navigation with human-agent interaction (e.g., DialFRED [3]). Among them, coarse-grained navigation with simple and concise instructions better aligns with our human practical needs.



Figure 1. There are three types of nodes, and different colors represent different types of regions. Our agent utilizes the proximity knowledge constructed from the auxiliary task during the navigation process and calculates the optimal path based on the MRNA. However, according to this path, the agent does not find the bathroom in the rec room, so it chooses the sub-optimal path and backtrack based on the semantic topological maps to finally find the target region.

Early research [1, 2, 4–6] employed recurrent neural network architectures like LSTM [7] to build agents. However, due to their relatively inefficient learning of long-term dependencies, these models struggle to effectively propagate navigation history information during recurrent steps. Recent studies [8–11], based on the transformer [12] architecture, utilize attention mechanisms to better model long-term dependencies between navigation actions and employ topological maps for global and local planning to achieve more efficient navigation. While they implicitly learn some knowledge beneficial for navigation, they still have limitations in terms of interpretability and learning efficiency, resulting in ineffective exploration of the environment to reach the target. As shown in Figure 1, in the absence of additional cues, most traditional agents, relying solely on information of vision and language, is likely to choose to enter the next new region, the kitchen, since the traversed regions have obtained relatively low visual scores. Only when the target region is observed can a higher visual score be obtained.

This indicates that the navigational exploration process among these traditional agents is often carried out in the absence of strong evidence. Some research [13, 14] introduces knowledge from concept-based or image-based knowledge bases [15, 16] to enhance generalization ability of the model and address the aforementioned issue. However, these methods have two limitations: 1. The knowledge bases used for knowledge extraction are not specifically constructed for navigation tasks, resulting in an inclusion of excessive knowledge irrelevant to navigation, which increases the difficulty of knowledge extraction. 2. Reasoning on knowledge has not been fully achieved, limiting the exploration of the potential value of the knowledge.

To address the aforementioned issues, we propose a Hierarchical Spatial Proximity Reasoning (HSPR) model, which leverages hierarchical spatial proximity knowledge about the navigation environment to perform multi-step reasoning on navigation paths, as illustrated in Figure 1. HSPR is pre-trained and then applied to navigation tasks. In order to construct hierarchical spatial proximity knowledge in the process of pre-training, we propose a Scene Understanding Auxiliary Task (SUAT) to uncover the adjacency relationships between regions, objects, and region-object pairs in the navigation environment, and utilize panoramic views and object features encoded by the multi-layer transformer to recognize each region in the navigation environment. Subsequently, we learn the prediction of proximity scores by combining the proximity score adaptive function designed in the Proximity Adaptive Attention Module (PAAM) with the attention mechanism.

For navigation, we propose a Multi-step Reasoning Navigation Algorithm (MRNA) that involves reasoning on proximity knowledge and advanced applications of hierarchical navigation strategies. This algorithm can plan several paths with the highest confidence from the current region to the target region, choose the next region of the optimal path as the sub-target, and calculate the region proximity scores of each navigable node on the semantic topological maps leading to the sub-target, then fuse it with its visual score to obtain the action scores for navigation decision. To accomplish this, we also introduce a Residual Fusion Method (RFM) to improve the accuracy of the fused action scores, and it exhibits better interpretability compared to traditional fusion methods.

In summary, the main contributions of this paper are as follows. (i) We propose a Scene Understanding Auxiliary Task (SUAT), enabling the agent to construct hierarchical spatial proximity knowledge directly from the navigation environment. (ii) We propose a Multi-step Reasoning Navigation Algorithm (MRNA) based on the semantic topological maps, allowing the agent to perform reasoning using hierarchical spatial proximity knowledge, exploring potential feasible paths, and achieving efficient hierarchical exploration and navigation decision-making.

(iii) The effectiveness of our proposed method has been extensively validated through extensive experimentation. The Hierarchical Spatial Proximity Reasoning (HSPR) model, with the aforementioned components at its core, has obtained satisfactory results on benchmark VLN datasets including REVERIE, SOON, R2R, and R4R.

## 2. Related work

**Visual and Language Navigation.** Since its introduction in [1], VLN has gained significant attention. This task holds great societal significance in areas such as social services, rescue operations, and healthcare. Progress in VLN has been made through innovations at various levels, including fine-grained [1, 17, 18] to coarse-grained [2, 19] instruction conversion, memory structure improvements from state vectors [5, 6] to topological maps [20–22], architectural upgrades from recurrent neural networks with cross-modal attention [1, 2, 4–6] to transformers [8–11, 13, 14], and continuous innovation in representation learning [8, 23, 24], navigation strategies [25–27], exploration and exploitation [28, 29], and data augmentation [6, 30–32]. Recently, most VLN methods [8, 24, 33, 34] have relied on large-scale pre-trained networks for encoding visual and language features. However, these methods did not explicitly utilize spatial proximity cues beyond the two input modalities, which are crucial for guiding the agent.

**Learning with Auxiliary Tasks.** Auxiliary tasks have played a crucial role in assisting agents to better understand the environment and their own state, leading to more efficient and robust predictions of future decision-making information [5, 35, 36]. For example, AuxRN [5] improves the internal state representation of the policy network through auxiliary tasks, enhancing the agent’s performance. SEA [35] enhances the visual representation of the environment by improving the image encoder through auxiliary tasks. Additionally, auxiliary tasks can also cover content relevant to the current task, such as monitoring task completion [37] and alignment between visual and navigation instructions [31]. Our proposed auxiliary task effectively uncovers adjacency relationships between regions, objects, and region-object pairs in the environment. This knowledge is then applied in subsequent navigation tasks, leading to a significant improvement in navigation efficiency.

**Vision-Language Reasoning.** The vision-language multi-modal tasks that connect computer vision and natural language processing have attracted significant attention, with visual-language reasoning playing a crucial role in these tasks. Recent studies [33, 38] have focused on obtaining higher-level semantics by pre-training models on large-scale datasets with visual language reasoning tasks such as VQA [39]. Other studies [4, 40] have employed cross-modal attention mechanisms to reason about visual entities. CLIP-NAV [41] employs CLIP [42] for zero-shot

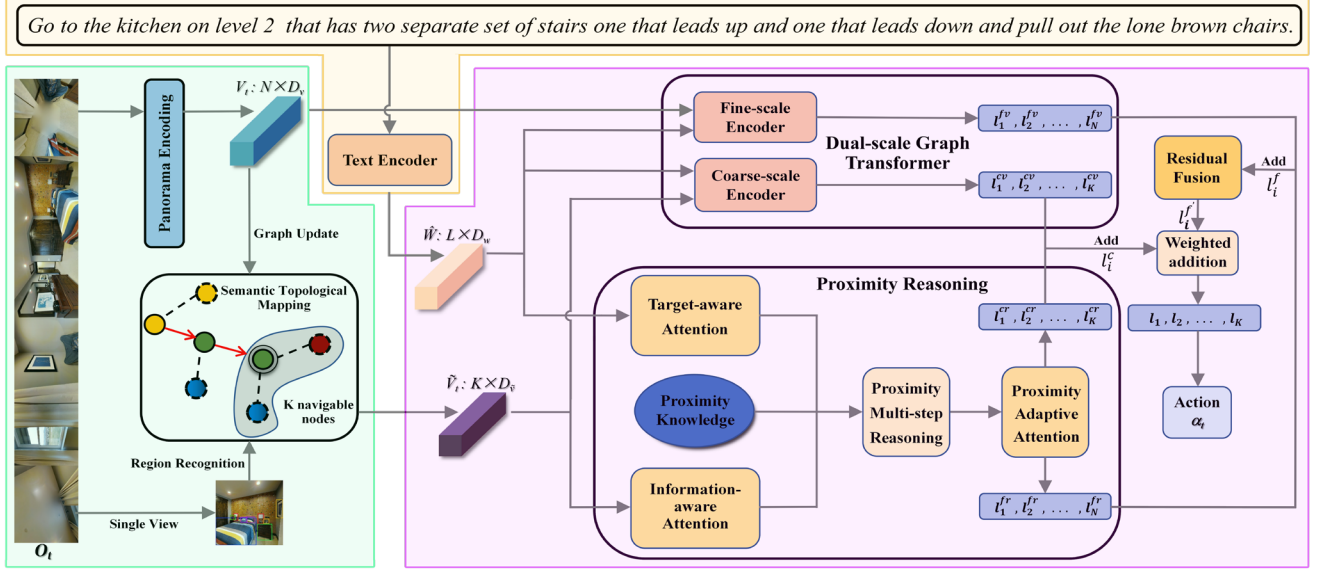


Figure 2. HSPR Architecture, including the Text Encoder, Semantic Topological Mapping, and Navigation Action Prediction modules. The Text Encoder encodes the navigation instructions, the Semantic Topological Mapping module progressively constructs and updates the semantic topological graph, and the Navigation Action Prediction module fuses the visual scores predicted by the Dual-scale Graph Transformer [11] with the region proximity scores predicted by the Proximity Reasoning module to obtain action scores. Best viewed in color.

cross-modal transfer. Furthermore, there are studies that combine additional knowledge bases for reasoning in navigation. For example, CKR [13] retrieves graph-structured knowledge related to room and object entities from ConceptNet [15]. KERM [14] leverages a knowledge base built from the Visual Genome dataset [16] to retrieve facts about navigation views, enabling a better understanding of visual concepts. In this work, we do not rely on knowledge extraction from external knowledge bases. Instead, we extract knowledge directly from the navigation environment and apply it to the reasoning of the navigation task.

### 3. Method

**Problem Formulation.** In the task of visual-language navigation in discrete environment, a navigation scene is represented as an undirected graph  $\mathcal{G} = \{\mathcal{V}, \mathcal{E}\}$ , where  $\mathcal{V}$  denotes the set of  $V$  nodes and  $\mathcal{E}$  represents the connecting edges. Each node is associated with a panoramic view  $\mathcal{P} = \{p_i\}_{i=1}^{36}$  divided into 36 parts, and each part  $p_i = \{v_i, o_i, \theta_i, \varphi_i\}$  contains image representation  $v_i$ , object representation  $o_i$ , heading angle  $\theta_i$ , and elevation angle  $\varphi_i$ . A region  $R = \{v_i\}_{i=0}^M$  is a collection of nodes of the same type, for two different regions  $A, B$ , if there exists a node in  $A$  with a candidate node set  $C$ , and  $C \cap B \neq \emptyset$ , then these two regions are connected. Navigable nodes are those that can be reached from previously visited nodes. The agent is initialized at a random location and receives an instruction  $\mathcal{W} = \{w_i\}_{i=1}^L$ , where  $L$  is the number of words

contained in the instruction. At each time step  $t$ , the agent observes a panoramic view  $\mathcal{P}_t$  of the current node. In addition, the agent knows its candidate nodes and the corresponding view set  $\mathcal{N}(V_t)$ . Subsequently, the agent needs to take an action of selecting a view from the set of candidate views  $\{v_{t,i}\}_{i=0}^N$ , where  $v_{t,0}$  represents the action to stop. After the agent decides to stop at a certain location, it also needs to predict the location of the target object in the panoramic view.

**Overview.** As shown in Figure 2, our model is built upon the architecture of Dual-scale Graph Transformer (DUET) [11], consisting of three components: the text encoder, the semantic topological mapping module, and the navigation action prediction module. Specifically, our model leverages proximity knowledge acquired from the Scene Understanding Auxiliary Task (SUAT) to guide the progressive update of the semantic topological map during the navigation process. Based on this, our model employs the Multi-step Reasoning Navigation Algorithm (MRNA) to plan several paths with the highest confidence and selects the next potential region as the sub-target from the optimal path. We calculate the region proximity scores of each navigable node with respect to the sub-target, which are fused with the visual scores predicted by the DUET. This fusion process yields more accurate action scores.

#### 3.1. Scene Understanding

To obtain common sense information and accurately predict region types for more precise navigation, we

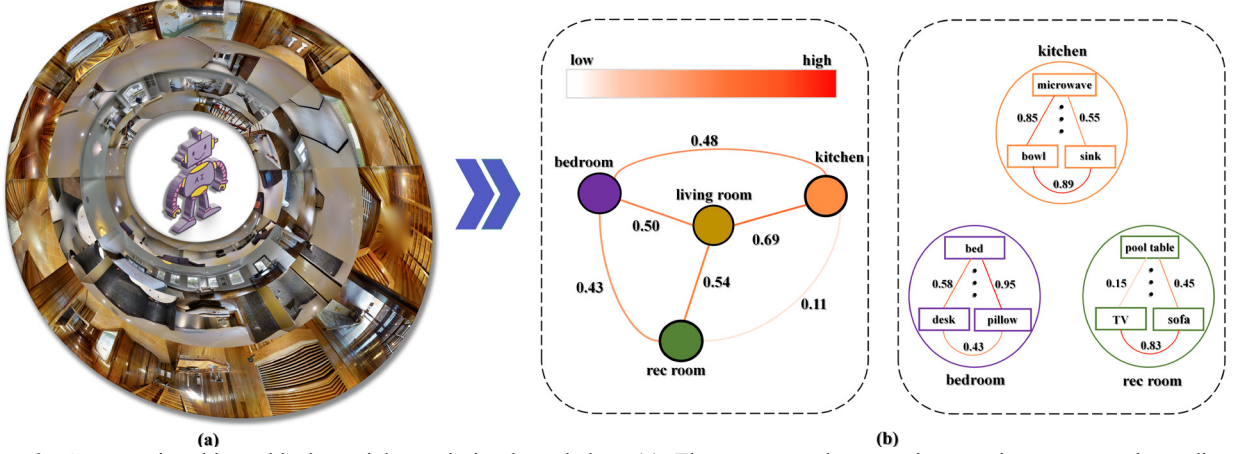


Figure 3. Constructing hierarchical spatial proximity knowledge. (a) The agent explores various regions, uncovering adjacency relationships between regions, objects, and spatial co-occurrence between regions and objects. (b) A portion of the hierarchical spatial proximity maps constructed by SUAT is shown. The left side shows the proximity probabilities between different regions, while the right side displays the highest K co-occurring objects within a specific region and their corresponding proximity probabilities.

propose a Scene Understanding Auxiliary Task (SUAT) that records the adjacency relationships in the navigation environment and trains the agent to recognize region types of nodes, as shown in Figure 3(a).

**Constructing Proximity Knowledge.** Firstly, we utilize the region types and object labels in the navigation scenes to obtain the region adjacency count matrix  $C^r \in \mathbb{R}^{N_r \times N_r}$ , the object adjacency count matrix  $C^o \in \mathbb{R}^{N_o \times N_o}$ , and the region-object correlation count matrix  $C^{ro} \in \mathbb{R}^{N_r \times N_o}$ , where  $N_r$  represents the number of region types and  $N_o$  represents the number of object types. Specifically, we segment each scene into different regions, and if there are multiple disconnected regions of the same type, we further divide them into multiple independent regions. We then count the connectivity between the segmented regions. For objects, we consider that there is adjacency between all objects in each view  $p_i$ , and the count of co-occurrence between them is plus one.

The adjacency probability matrix obtained by simple normalization of adjacency count matrix is not accurate and leads to inefficient navigation. Considering the extreme values in the adjacency count matrix, we elaborately design a normalization function:

$$P_{i,j} = \begin{cases} -\frac{C_{i,j}^2}{2a_i^2} + \frac{C_{i,j}}{a_i}, & C_{i,j} < a_i \\ \frac{C_{i,j}^2 + a_i^2 - 2a_i C_{i,j}}{2(a_i - m_i)^2} + 0.5, & C_{i,j} \geq a_i \end{cases} \quad (1)$$

where  $a_i$  represents the average count of matrix  $C$  in the  $i$ -th row after excluding the two maximum and two minimum values, and  $m_i$  is the maximum value in the  $i$ -th row of matrix  $C$  (after the exclusion operation) plus  $a_i$ . Finally, to extract spatial co-occurrence knowledge between regions and objects, we also identify the K objects that co-occur most frequently with each region. The resulting adjacency knowledge is illustrated in Figure 3(b). For more visualizations of knowledge, detailed

methodology, and images of normalization functions, please refer to the appendix.

**Region Recognition.** The agent encodes and models the visual representation  $v_{t,i}$  and the object set representation  $o_{t,i}$  of each navigable node using a multi-layer transformer [12]. Subsequently, the output of the FC layer yields the region type score  $S_{t,i}^r \in \mathbb{R}^{1 \times N_r}$  for the respective node. The prediction task is formulated as a classification problem, and the calculation of region type score  $S_{t,i}^r$  is as follows:

$$[v'_{t,i}; o'_{t,i}] = \sum_i \sigma([v_{t,i}; o_{t,i}] W_s h_{t-1}^T) [v_{t,i}; o_{t,i}] \quad (2)$$

$$S_{t,i}^r = \sigma(FC([v'_{t,i}; o'_{t,i}])) \quad (3)$$

where  $\sigma$  is the softmax activation function (used in subsequent formulas),  $W_s \in \mathbb{R}^{D_v \times D_h}$  is a learnable parameter,  $h_{t-1} \in \mathbb{R}^{1 \times D_h}$  is the hidden state of the transformer decoder at time step  $t-1$ , and we continue to use  $v_{t,i}, o_{t,i}$  instead of  $v'_{t,i}, o'_{t,i}$  to represent the encoded embedding later on. The loss function for region classification is cross-entropy:

$$L_r = \sum_{t=1}^T \sum_{i=1}^{N_r} (-\log s_{t,i}^{\hat{r}_{t,i}}) \quad (4)$$

where  $\hat{r}_{t,i}$  represents the ground truth room-type of each node.

### 3.2. Proximity Reasoning

To better utilize the hierarchical spatial proximity knowledge, we propose the HSPR model as depicted in Figure 2. Specifically, we extract region type representations from semantic topological nodes  $v_{t,i}$  and the instruction  $\hat{w}_i$  using the attention mechanism. Leveraging the constructed proximity knowledge, we perform multi-step proximity calculations to realize the reasoning process. Furthermore, we fuse the visual scores

predicted by the DUET [11] with the region proximity scores through residual fusion.

**Proximity Calculating.** We input the feature representation  $v_{t,i}$  of navigable nodes in the semantic topological maps to the information-aware attention module. This module calculates the region type representation of navigable nodes and the object representation contained in the stop node via:

$$R_{t,i} = \sigma(FC(\sum_i \sigma(v_{t,i} W_{vr} h_{t-1}^T) v_{t,i})) \quad (5)$$

$$O_{n,i} = \sigma(FC(\sum_i \sigma(v_{n,i} W_{vo} h_{n-1}^T) v_{n,i})) \quad (6)$$

where  $W_{vr}$  and  $W_{vo}$  are learnable parameters, and  $h_{t-1}$ ,  $h_{n-1}$  are the hidden state of the transformer decoder at  $t-1$  and penultimate time steps respectively. Next, we input the instruction embedding  $\hat{w}_i$  into the target-aware attention layer to obtain the representations of the target region and target object via:

$$T_t^r = \sigma(FC(\sum_i \sigma(\hat{w}_i W_r h_{t-1}^T) \hat{w}_i)) \quad (7)$$

$$T_n^o = \sigma(FC(\sum_i \sigma(\hat{w}_i W_o h_{n-1}^T) \hat{w}_i)) \quad (8)$$

where  $W_r$  and  $W_o$  are learnable parameters.

Building upon this, we leverage the constructed proximity knowledge to compute the region proximity scores between the current navigable nodes and the target region, as well as the object proximity scores between various objects and the target object at the stopping moment:

$$l_{t,i}^r = R_{t,i} P^r T_t^{rT} \quad (9)$$

$$l_{n,i}^o = O_{n,i} P^o T_n^{oT} \quad (10)$$

where  $P^r$  and  $P^o$  represent the region and object proximity probability matrix obtained from the auxiliary task respectively.

**Multi-step Reasoning.** The initial position of the agent is often not adjacent to the target region, resulting in a low or even zero score for the proximity of each navigable node to the target. However, the agent can cleverly utilize these nodes as intermediate stations to gradually approach the target region until it successfully reaches the final destination.

Based on this intuition, we propose a Multi-Step Reasoning Navigation Algorithm (MRNA) that allows the agent to continuously plan multiple feasible paths from one region to another, as illustrated in Figure 4. It is at each time step  $t$  that the agent reasons about the top  $K$  candidate paths with the highest confidence and selects the optimal path. This is because during the progressive construction of the semantic topological map, nodes of new region types are continuously added, and the agent must always ensure that the current path is the optimal path. In the estimated paths, the next potential region is treated as the sub-target. If no sub-target is found, the agent selects the next-best path until all sub-targets are found and the target region is reached. The calculation of the region proximity scores for the  $i$ -th navigable node is as follows:

$$l_{t,i}^{r*} = \gamma^0 w_1 l_{t,i}^{r(1)} + \gamma^1 w_2 l_{t,i}^{r(2)} + \dots + \gamma^{n-1} w_n l_{t,i}^{r(n)} \quad (11)$$

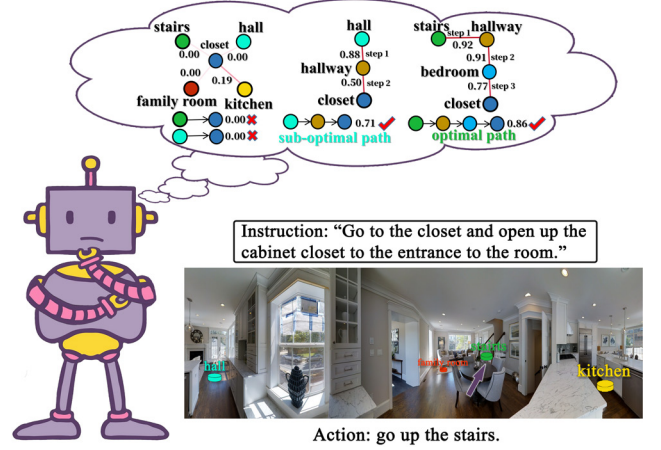


Figure 4. Multi-step reasoning navigation example. Despite the low probabilities of the current navigable nodes leading directly to the target region, the intelligent agent utilizes the MRNA to plan multiple feasible paths. From these paths, the agent selects the optimal path, which involves going through the staircase, hallway, and bedroom to reach the target region.

where  $\gamma$  is the discount factor,  $W \in \mathbb{R}^{1 \times n}$  is the weight coefficient,  $l_{t,i}^{r(n)}$  represents the score of region proximity obtained from the  $n$ -th step reasoning calculation.

### 3.3. Proximity Adaptive Attention Module

To obtain proximity scores that can better integrate with the visual scores and object scores predicted by DUET [11], we propose the Adjacency Adaptive Attention Module. Specifically, in the pre-training task of Single-step Action Prediction (SAP) [10] (which will be introduced in Sec 3.5), we utilize dot-product attention to predict two key parameters: the activation threshold  $t_0$  and the scaling factor  $s_0$ :

$$t_0 = m(\sigma(\hat{v}_0^c W_q (\hat{v}_0^c W_k)^T)) \quad (12)$$

$$s_0 = m(\sigma([\hat{v}_0^c; \hat{v}_0^f] W_q ([\hat{v}_0^c; \hat{v}_0^f] W_k)^T)) \quad (13)$$

where  $m$  represents the mean function,  $W_*$  is a learnable parameter,  $\hat{v}_0^c$  and  $\hat{v}_0^f$  are embeddings for global and local stop actions, respectively. Then we design a proximity score adaptive function:

$$l_i' = \begin{cases} \frac{s_0}{1-t_0} l_i^* + \frac{s_0 t_0}{t_0 - 1}, & l_i^* \geq t_0 \\ \frac{s_0}{t_0} l_i^* - s_0, & l_i^* < t_0 \end{cases} \quad (14)$$

This makes the upper and lower limits of proximity scores related to  $s_0$ . The probability values lower than  $t_0$  will receive negative scores. We will still use  $l_i$  instead of  $l_i'$  to indicate proximity scores.

### 3.4. Residual Fusion

In the process of converting local action scores  $l_i^f \in \{v_i\}_{i=0}^N$  to global action scores  $l_i^c \in \{v_i\}_{i=0}^K$ , we employ a novel score fusion method called residual fusion.

We refer to all nodes in the global navigable nodes except the local navigable nodes as non-overlapping navigable nodes. The practice of simply adding up the action scores of visited nodes and assigning them to non-overlapping navigable nodes, as presented in Dynamic Fusion [11], is not accurate. This is because there is no direct relation between these visited nodes and non-overlapping navigable nodes. In contrast, our residual fusion method combines the global region proximity scores of nodes with their global visual scores and assigns them to the non-overlapping navigable nodes. This approach effectively utilizes proximity knowledge and provides more accurate estimates of action scores:

$$l_i' = \begin{cases} l_i^f, & \text{if } V_i \in \{v_i\}_{i=0}^N, \\ l_i^{cr} + l_i^{cv}, & \text{otherwise.} \end{cases} \quad (15)$$

Finally, we add the local action scores after residual fusion with the global action scores by weight to obtain the final action scores.

### 3.5. Training and Inference

**Pre-training.** In previous studies [8, 24, 33, 34, 38], it has been demonstrated that pre-training techniques significantly improve model performance. To pre-train the VLN model, this study adopts Masked Language Modeling (MLM) [43] for language encoder pre-training. Additionally, Masked Region Classification (MRC) [33], Single-step Action Prediction (SAP) [10], and Object Grounding (OG) [44] methods are used to enhance the pre-training of the visual encoder. Compared to DUET [11], we additionally predict two key coefficients in SAP, namely the activation threshold and scaling factor mentioned in Sec 3.3. The imitation learning with SAP and OG losses for a given demonstrated path  $P^*$  is as follows:

$$L_{SAP} = \sum_{t=1}^T -\log p(a_t^* | \mathcal{W}, P_{<t}^*) \quad (16)$$

$$L_{OG} = \sum_{t=1}^T -\log p(o^* | \mathcal{W}, P_D) \quad (17)$$

where  $a_t^*$  represents the expert action for the partial demonstration path  $P_{<t}^*$ , and  $o^*$  is the ground truth object at the final location  $P_D$ . More details are presented in the appendix.

**Fine-tuning and Inference.** In order to further fine-tune the model, we integrate the pseudo interactive demonstrator (PID) [11], where the loss function  $L_{PID}$  follows the same structure as the SAP loss in pre-training. However,  $a_t^*$  is replaced with the pseudo expert action of selecting the navigable node with the shortest total distance from the current node to the destination, and the

demonstrated path  $P^*$  is replaced with a trajectory sampled based on the current policy.

During the navigation process, the model predicts an action for each step. If the action is not a stop action, the agent uses the Floyd algorithm to plan the optimal path based on the constructed semantic topological maps and moves to the predicted node. Otherwise, the agent stops at the current node. If the agent exceeds the maximum number of steps set, it is forcibly terminated and moves to the node with the highest stop action score as the final predicted location. At this node, the agent selects the object with the highest prediction score as its target.

## 4. Experiment

### 4.1. Datasets and Evaluation Metrics

**Datasets.** We evaluated our model on four VLN benchmark datasets based on the Matterport3D [45] dataset: R2R [1], R4R [17], REVERIE [2], and SOON [19]. The region types of all nodes in each scene and the object information contained in  $p_i$  in the associated panorama  $\mathcal{P} = \{p_i\}_{i=1}^{36}$  are marked in the Matterport3D dataset. The focus of the evaluation was on REVERIE and SOON, both of which are goal-oriented VLN benchmark datasets. REVERIE includes high-level instructions with an average length of 21 words. Unlike the other three datasets, when the agent navigates to the target location based on coarse-grained instructions, it also needs to select the bounding box of the target object. The instructions in the SOON dataset have an average length of 47 words and also describe information about objects near the target and the location of the target room. The R2R dataset provides step-by-step instructions, describing detailed references for each step, with an average length of 32 words. The R4R dataset combines paths from the R2R dataset to create longer and more complex routes.

**Evaluation Metrics.** We use standard metrics [1] to measure navigation performance, including Trajectory Length (TL): the average path length in meters, Navigation Error (NE): the average distance between the final position of agent and the target in meters, Success Rate (SR): the proportion of paths with NE less than 3 meters, Oracle Success Rate (OSR): SR given an oracle stop policy, Success weighted by Path Length (SPL): SR penalized by path length. To evaluate object grounding, we use Remote Grounding Success (RGS) [2]: the proportion of successfully executed instructions, RGS weighted by Path Length (RGSPL): RGS penalized by path length. Except for TL and NE, higher values are better for all metrics.

### 4.2. Implementation Details

**Model Architectures.** The dimension of the counting matrix is  $N_r = 31$ , and  $N_o = 1600$ . The dimension of the

Methods	Val Seen						Val Unseen						Test Unseen					
	Navigation			Grounding			Navigation			Grounding			Navigation			Grounding		
	TL ↓	OSR ↑	SR ↑	SPL ↑	RGS ↑	RGSPL ↑	TL ↓	OSR ↑	SR ↑	SPL ↑	RGS ↑	RGSPL ↑	TL ↓	OSR ↑	SR ↑	SPL ↑	RGS ↑	RGSPL ↑
Human	-	-	-	-	-	-	-	-	-	-	-	-	21.18	86.83	81.51	53.66	77.84	51.44
Seq2Seq [1]	12.88	35.70	29.59	24.01	18.97	14.96	11.07	8.07	4.20	2.84	2.16	1.63	10.89	6.88	3.99	3.09	2.00	1.58
SMNA [37]	7.54	43.29	41.25	39.61	30.07	28.98	9.07	11.28	8.15	6.44	4.54	3.61	9.23	8.39	5.80	4.53	3.10	2.39
CKR [13]	12.16	61.91	57.27	53.57	39.07	-	26.26	31.44	19.14	11.84	11.4	-	22.46	30.40	22.00	14.25	11.60	-
VLNBERT [24]	13.44	53.90	51.79	47.96	38.23	35.61	16.78	35.02	30.67	24.90	18.77	15.27	15.68	32.91	29.61	23.99	16.50	13.51
HAMT [10]	12.79	47.65	43.29	40.19	27.20	15.18	14.08	36.84	32.95	30.20	18.92	17.28	13.62	33.41	30.40	26.67	14.88	13.08
Airbert [34]	15.16	49.98	47.01	42.34	32.75	30.01	18.71	34.51	27.89	21.88	18.23	14.18	17.91	34.20	30.28	23.61	16.83	13.28
DUET [11]	13.86	73.68	71.75	63.94	57.41	51.14	22.11	51.07	46.98	33.73	32.15	23.03	21.30	56.91	52.51	36.06	31.88	22.06
KERM [14]	12.84	79.20	76.88	<b>70.45</b>	61.00	56.07	21.85	55.21	50.44	35.38	34.51	24.45	17.32	57.58	52.43	39.21	32.39	23.64
STPR(Ours)	13.66	<b>80.60</b>	<b>77.16</b>	70.17	<b>62.47</b>	<b>56.77</b>	23.24	<b>59.16</b>	<b>53.25</b>	<b>38.19</b>	<b>37.80</b>	<b>27.25</b>	19.22	<b>59.60</b>	<b>54.38</b>	<b>39.41</b>	<b>34.73</b>	<b>23.95</b>

Table 1. Comparison with SOTA methods on REVERIE dataset.

Methods	Val Seen House				Unseen House (Test)			
	OSR ↑	SR ↑	SPL ↑	RGSPL ↑	OSR ↑	SR ↑	SPL ↑	RGSPL ↑
Human	-	-	-	-	91.4	90.4	59.2	51.1
Random	0.4	0.1	0.0	0.9	2.7	2.1	0.4	0.0
Speaker-Follower [6]	69.4	61.2	60.4	9.1	9.8	7.0	6.1	0.6
AuxRN [5]	78.5	68.8	67.3	8.3	11.0	8.1	6.7	0.5
GBE w/o GE	73.0	62.5	60.8	6.7	18.8	11.4	8.7	0.8
GBE [19]	64.1	76.3	62.5	7.3	19.5	11.9	10.2	1.4
DUET <sup>†</sup>	80.3	78.2	69.5	11.9	43.0	33.4	21.4	4.2
STPR(Ours)	<b>84.7</b>	<b>80.4</b>	<b>70.2</b>	<b>12.2</b>	<b>53.4</b>	<b>39.1</b>	<b>27.3</b>	<b>4.7</b>

Table 2. Comparison with SOTA methods on SOON dataset. <sup>†</sup> indicates reproduced results.

feature channels is set to  $D_v = D_h = 768$ . The number of transformer layers for instructions, visual, and local-global cross-modal attention modules are set to 9, 2, 4 and 4, respectively. The discount factor  $\gamma$  for multi-step reasoning is set to 0.9. We initialize the model using the pre-trained LXMERT [40] and utilize the ViT-B/16 [46] pre-trained model to extract image features. ViT-B/16 also provides object bounding box information for the REVERIE dataset, enabling object detection on this dataset. For the SOON dataset, we employ the BUTD object detector [4] for object detection.

**Training Details.** During the pre-training process, we used 4 NVIDIA RTX 3080 GPU and set the batch size to 16. For the REVERIE dataset, we pre-trained our model for 100,000 iterations. Then, we fine-tuned the pre-trained model for 20,000 iterations with a batch size of 8 on 1 NVIDIA RTX 3080 GPU. For the SOON dataset, we pre-trained the model for 40,000 iterations. Then, we fine-tuned the pre-trained model for 20,000 iterations with a batch size of 2. For the R2R dataset, we pre-trained the model for 200,000 iterations. Then, we fine-tuned the pre-trained model for 20,000 iterations with a batch size of 8. The training settings for the R4R dataset are the same as the R2R dataset. For all datasets, we selected the best epoch based on the SPL metric on the val unseen split.

### 4.3. Comparison with SOTA Methods

**REVERIE, SOON.** Tables 1, 2 present the results of

Methods	Val Unseen				Test Unseen			
	TL ↓	NE ↓	SR ↑	SPL ↑	TL ↓	NE ↓	SR ↑	SPL ↑
Seq2Seq [1]	8.93	7.81	21	-	8.13	7.85	20	18
EnvDrop [30]	10.7	5.22	52	48	11.6	5.23	51	47
AuxRN [5]	-	5.28	54	50	-	5.15	55	51
SSM [22]	20.7	4.32	62	45	20.4	4.57	61	46
VLNBERT [24]	12.01	3.93	63	57	12.35	4.09	63	57
HAMT-e2e [10]	11.46	<b>2.29</b>	66	61	12.27	3.93	65	60
DUET [11]	13.94	3.31	71.52	60.42	14.73	3.65	69.25	58.68
KERM [14]	13.54	3.22	71.95	60.91	14.60	3.61	69.73	<b>59.25</b>
STPR(Ours)	13.81	3.05	<b>73.61</b>	<b>62.70</b>	15.82	<b>3.60</b>	<b>70.29</b>	59.19

Table 3. Comparison with SOTA methods on R2R dataset.

Methods	Val Seen				Val Unseen			
	TL ↓	NE ↓	SR ↑	SPL ↑	TL ↓	NE ↓	SR ↑	SPL ↑
Random	21.80	11.40	13	2	23.60	10.40	14	2
Speaker-Follower [6]	15.40	5.35	52	37	19.90	8.47	24	12
RCM+goal oriented [25]	24.50	5.11	56	32	32.50	8.45	29	10
RCM+fidelity oriented	18.80	5.37	53	31	28.50	8.08	26	8
PTA low-level [47]	11.90	5.11	57	45	10.20	8.19	27	15
PTA high-level	16.50	4.54	58	39	17.70	8.25	24	10
EnvDrop [30]	19.85	-	52	41	26.97	-	29	18
OAAAM [48]	11.75	-	56	49	13.80	-	31	23
SSM [22]	19.40	4.60	63	-	22.10	<b>3.22</b>	32	-
DUET <sup>†</sup>	18.63	4.38	63.00	60.11	23.02	6.40	45.11	40.62
STPR(Ours)	17.83	<b>4.04</b>	<b>65.70</b>	<b>61.84</b>	22.09	5.94	<b>47.89</b>	<b>43.65</b>

Table 4. Comparison with SOTA methods on R4R dataset. <sup>†</sup> indicates reproduced results.

HSPR on the REVERIE and SOON datasets, respectively. Our approach achieves the best results on most metrics in both datasets. As shown in Table 1, compared to the baseline, our method achieves improvements of at least 2.81% in SR and 2.81% in SPL on the val unseen split of REVERIE. On the test unseen split, we observe improvements of at least 1.95% in SR and 0.20% in SPL. For the SOON dataset, as evident in Table 2, HSPR outperforms other baselines significantly in the test unseen split, with a 5.7% increase in SR and a 5.9% increase in SPL. These results demonstrate that HSPR can effectively perform reasoning-based navigation without detailed step-by-step instruction guidance, leveraging proximity knowledge. Visual demonstrations and analysis of successful or failed HSPR navigation cases refer to the qualitative examples in the appendix.

**R2R, R4R.** Table 3, 4 present the results of HSPR on the R2R and R4R datasets, respectively. On the R2R dataset, our method achieves improvements of 1.66% and 0.56% in SR, and 1.79% and 0.06% in SPL on the val unseen and test unseen split, respectively. On the R4R dataset, we observe improvements of 2.70% and 2.78% in SR, and 1.73% and 3.03% in SPL on the val seen and val unseen split, respectively. The model’s performance on R2R is significantly lower compared to that on REVERIE, while it continues to perform well on R4R. We attribute this to the fact that R2R involves fine-grained navigation instructions, where the key to successful navigation lies in aligning the agent’s trajectory with the instructions, with the proximity reasoning playing a supporting role. On the other hand, R4R, despite also having fine-grained navigation instructions, features longer navigation paths, enabling the MRNA to effectively demonstrate its capabilities.

#### 4.4. Ablation Study

We conducted extensive ablation experiments on the REVERIE dataset to investigate the contributions of each component to the navigation performance. All the results in this section are reported on the unseen split.

**Proximity knowledge.** We first compared the impact of proximity knowledge obtained from different methods on navigation. As shown in Table 5, the row 1 represents the baseline without any proximity knowledge. The row 2 shows the results obtained by utilizing proximity knowledge retrieved from the ConceptNet knowledge base [15]. Clearly, the results in the second row outperform those in the row 1, indicating that proximity knowledge can indeed improve navigation efficiency. The row 3 demonstrates the results obtained by utilizing proximity knowledge constructed from the SUAT proposed in this paper, which outperforms the previous two rows, suggesting that proximity knowledge obtained from the auxiliary task aligns better with the navigation environment. The row 4,5 employ PAAM to adaptively adjust the scores generated based on these two types of proximity knowledge. The improvement in navigation performance indicates that PAAM can effectively learn the prediction of proximity scores.

**Multi-step Reasoning Navigation.** The number of steps in multi-step reasoning corresponds to the maximum length of the reasoning path, which means the maximum number of regions that the agent will pass through. As shown in Table 6, performing multi-step reasoning navigation allows for better utilization of constructed proximity knowledge and the exploration of potential feasible paths, resulting in efficient navigation. For example, three-step reasoning improves the SPL to the highest value of 38.19%. However, as the number of reasoning steps increases, the performance starts to decline.

ConceptNet	SUAT	PAAM	OSR↑	SR↑	SPL↑	RGS↑	RGSPL↑
×	×	×	51.07	46.98	33.73	32.15	23.03
✓	×	×	54.93	48.99	34.30	33.14	23.37
×	✓	×	<b>60.83</b>	51.63	36.88	35.44	25.69
✓	×	✓	57.97	51.80	36.72	35.64	25.20
×	✓	✓	59.16	<b>53.25</b>	<b>38.19</b>	<b>37.80</b>	<b>27.25</b>

Table 5. Ablations of proximity knowledge and utilization on REVERIE val unseen split.

Step	OSR↑	SR↑	SPL↑	RGS↑	RGSPL↑
1	57.14	51.41	37.68	34.42	25.28
2	<b>61.57</b>	<b>54.56</b>	37.71	37.18	26.36
3	59.16	53.25	<b>38.19</b>	<b>37.80</b>	<b>27.25</b>
4	57.71	52.54	37.88	35.39	25.65
5	56.32	50.38	35.16	34.19	23.81

Table 6. The effect of the number of inference steps in MRNA on REVERIE val unseen split.

Fusion	OSR↑	SR↑	SPL↑	RGS↑	RGSPL↑
average	58.48	50.16	35.08	34.88	24.69
dynamic	58.25	52.34	37.43	35.33	25.53
residual	<b>59.16</b>	<b>53.25</b>	<b>38.19</b>	<b>37.80</b>	<b>27.25</b>

Table 7. Compare the performance of three different fusion methods on REVERIE val unseen split.

We believe that this is because the conditions for the existence of regions inferred at each step must be satisfied by existence of the regions inferred in the previous step. Consequently, the regions inferred in the fourth and fifth steps may appear illusory.

**Score Fusion Policy.** In Table 7, we compare three fusion methods: average fusion, dynamic fusion, and the proposed residual fusion. Compared to the first two fusion methods, the residual fusion improves SR by at least 0.91% and SPL by 0.76%.

## 5. Conclusion

This paper proposes a Hierarchical Spatial Proximity Reasoning (HSPR) model for the visual-and-language navigation (VLN) task. We design a Scene Understanding Auxiliary Task (SUAT) to identify regions in the scene during the interaction between the agent and the navigation environment, explore adjacency relationships, and construct hierarchical spatial proximity knowledge. Based on this, we propose a Multi-step Reasoning Navigation Algorithm (MRNA) that continuously infers optimal paths to the target region using proximity knowledge during the navigation process. Our approach achieves superior performance on the REVERIE, SOON, R2R, and R4R datasets, further demonstrating that knowledge-based reasoning navigation is an important means of breaking through VLN performance. We plan to apply HSPR to continuous environments in future work, and the code will be made publicly available to facilitate future research.

## References

- [1] Peter Anderson, Qi Wu, Damien Teney, Jake Bruce, Mark Johnson, Niko Sünderhauf, Ian Reid, Stephen Gould, and Anton van den Hengel. Vision-and-language navigation: Interpreting visually-grounded navigation instructions in real environments. In *CVPR*, pages 3674–3683, 2018. 1, 2, 6, 7
- [2] Yuankai Qi, Qi Wu, Peter Anderson, Xin Wang, William Yang Wang, Chunhua Shen, and Anton van den Hengel. Reverie: Remote embodied visual referring expression in real indoor environments. In *CVPR*, pages 9982–9991, 2020. 1, 2, 6, 7, 12
- [3] Xiaofeng Gao, Qiaozi Gao, Ran Gong, Kaixiang Lin, Govind Thattai, and Gaurav S Sukhatme. Dialfred: Dialogue-enabled agents for embodied instruction following. *arXiv preprint arXiv: 2202.13330*, 2022. 1
- [4] Peter Anderson, Xiaodong He, Chris Buehler, Damien Teney, Mark Johnson, Stephen Gould, and Lei Zhang. Bottom-up and top-down attention for image captioning and visual question answering. In *CVPR*, pages 6077–6086, 2018. 1, 2, 3, 7, 11
- [5] Fengda Zhu, Yi Zhu, Xiaojun Chang, and Xiaodan Liang. Vision-language navigation with self-supervised auxiliary reasoning tasks. In *CVPR*, pages 10012–10022, 2020. 1, 2, 7
- [6] Daniel Fried, Ronghang Hu, Volkan Cirik, Anna Rohrbach, Jacob Andreas, Louis-Philippe Morency, Taylor Berg-Kirkpatrick, Kate Saenko, Dan Klein, and Trevor Darrell. Speaker-follower models for vision-and-language navigation. In *NeurIPS*, pages 3318–3329, 2018. 1, 2, 7
- [7] S. Hochreiter and J. Schmidhuber. Long short-term memory. *Neural computation*, 9(8):1735–1780, 1997. 1
- [8] Alexander Pashevich, Cordelia Schmid, and Chen Sun. Episodic transformer for vision-and-language navigation. In *ICCV*, pages 15942–15952, 2021. 1, 2, 6, 7
- [9] Kevin Chen, Junshen K Chen, Jo Chuang, Marynel Vázquez, and Silvio Savarese. Topological planning with transformers for vision-and-language navigation. In *CVPR*, pages 11276–11286, 2021. 1, 2
- [10] Shizhe Chen, Pierre-Louis Guhur, Cordelia Schmid, and Ivan Laptev. History aware multimodal transformer for vision-and-language navigation. In *NeurIPS*, pages 5834–5847, 2021. 1, 2, 5, 6, 7
- [11] Shizhe Chen, Pierre-Louis Guhur, Makarand Tapaswi, Cordelia Schmid, and Ivan Laptev. Think global, act local: Dual-scale graph transformer for vision-and-language navigation. In *CVPR*, pages 16537–16547, 2022. 1, 2, 3, 5, 6, 7, 11, 12, 13
- [12] Ashish Vaswani, Noam Shazeer, Niki Parmar, Jakob Uszkoreit, Llion Jones, Aidan N Gomez, Łukasz Kaiser, and Illia Polosukhin. Attention is all you need. In *NeurIPS*, pages 5998–6008, 2017. 1, 4
- [13] Chen Gao, Jinyu Chen, Si Liu, Luting Wang, Qiong Zhang, and Qi Wu. Room-and object aware knowledge reasoning for remote embodied referring expression. In *CVPR*, pages 3064–3073, 2021. 2, 3, 7
- [14] Xiangyang Li, Zihan Wang, Jiahao Yang, Yaowei Wang, and Shuqiang Jiang. Kerm: Knowledge enhanced reasoning for vision-and-language navigation. In *CVPR*, pages 2583–2592, 2023. 2, 3, 7
- [15] Robyn Speer, Joshua Chin, and Catherine Havasi. Conceptnet 5.5: An open multilingual graph of general knowledge. In *AAAI*, pages 4444–4451, 2017. 2, 3, 8
- [16] Ranjay Krishna, Yuke Zhu, Oliver Groth, Justin Johnson, Kenji Hata, Joshua Kravitz, Stephanie Chen, Yannis Kalantidis, Li-Jia Li, David A Shamma, et al. Visual genome: Connecting language and vision using crowd sourced dense image annotations. *IJCV*, 123(1):32–73, 2017. 2, 3, 11
- [17] Vihan Jain, Gabriel Magalhaes, Alexander Ku, Ashish Vaswani, Eugene Ie, and Jason Baldridge. Stay on the path: Instruction fidelity in vision-and-language navigation. In *ACL*, pages 1862–1872, 2019. 2, 6
- [18] Alexander Ku, Peter Anderson, Roma Patel, Eugene Ie, and Jason Baldridge. Room-Across-Room: Multilingual vision-and-language navigation with dense spatiotemporal grounding. In *EMNLP*, pages 4392–4412, 2020. 2
- [19] Fengda Zhu, Xiwen Liang, Yi Zhu, Qizhi Yu, Xiaojun Chang, and Xiaodan Liang. Soon: Scenario oriented object navigation with graph-based exploration. In *CVPR*, pages 12689–12699, 2021. 2, 6, 7
- [20] Nikolay Savinov, Alexey Dosovitskiy, and Vladlen Koltun. Semi-parametric topological memory for navigation. In *ICLR*, 2018. 2
- [21] Devendra Singh Chaplot, Ruslan Salakhutdinov, Abhinav Gupta, and Saurabh Gupta. Neural topological slam for visual navigation. In *CVPR*, pages 12875–12884, 2020. 2
- [22] Hanqing Wang, Wenguan Wang, Wei Liang, Caiming Xiong, and Jianbing Shen. Structured scene memory for vision-language navigation. In *CVPR*, pages 8455–8464, 2021. 2, 7
- [23] Ronghang Hu, Daniel Fried, Anna Rohrbach, Dan Klein, Trevor Darrell, and Kate Saenko. Are you looking? grounding to multiple modalities in vision-and-language navigation. In *ACL*, pages 6551–6557, 2019. 2
- [24] Yicong Hong, Qi Wu, Yuankai Qi, Cristian Rodriguez-Opazo, and Stephen Gould. Vln bert: A recurrent vision-and-language bert for navigation. In *CVPR*, pages 1643–1653, 2021. 2, 6, 7
- [25] Xin Wang, Qiuyuan Huang, Asli Celikyilmaz, Jianfeng Gao, Dinghan Shen, Yuan Fang Wang, William Wang, and Lei Zhang. Reinforced cross-modal matching and self-supervised imitation learning for vision-language navigation. In *CVPR*, pages 6629–6638, 2019. 2, 7
- [26] Hanqing Wang, Wenguan Wang, Tianmin Shu, Wei Liang, and Jianbing Shen. Active visual information gathering for vision-language navigation. In *ECCV*, pages 307–322, 2020. 2
- [27] Jing Yu Koh, Honglak Lee, Yinfei Yang, Jason Baldridge, and Peter Anderson. Pathdreamer: A world model for indoor navigation. In *ICCV*, pages 14738–14748, 2021. 2
- [28] Amin Parvaneh, Ehsan Abbasnejad, Damien Teney, Qinfeng Shi, and Anton van den Hengel. Counterfactual vision-and-language navigation: Unravelling the unseen. In *NeurIPS*, pages 5296–5307, 2020. 2
- [29] Gunnar A. Sigurdsson, Jesse Thomason, Gaurav S. Sukhatme, and Robinson Piramuthu. Rrex-bot: Remote referring expressions with a bag of tricks. *arXiv preprint arXiv:2301.12614*, 2023. 2
- [30] Hao Tan, Licheng Yu, and Mohit Bansal. Learning to navigate unseen environments: Back translation with

- environmental dropout. In *NAACL*, pages 2610–2621, 2019. 2, 7
- [31] Haoshuo Huang, Vihan Jain, Harsh Mehta, Alexander Ku, Gabriel Magalhaes, Jason Baldridge, and Eugene Ie. Transferable representation learning in vision-and-language navigation. In *ICCV*, pages 7404–7413, 2019. 2
- [32] Ming Zhao, Peter Anderson, Vihan Jain, Su Wang, Alexander Ku, Jason Baldridge, and Eugene Ie. On the evaluation of vision-and-language navigation instructions. In *ACL*, pages 1302–1316, 2021. 2
- [33] Jiasen Lu, Dhruv Batra, Devi Parikh, and Stefan Lee. Vilbert: Pre-training task-agnostic visiolinguistic representations for vision-and-language tasks. In *NeurIPS*, volume 32, 2019. 2, 3, 6
- [34] Pierre-Louis Guhur, Makarand Tapaswi, Shizhe Chen, Ivan Laptev, and Cordelia Schmid. Airbert: In-domain pre-training for vision-and-language navigation. In *ICCV*, pages 1634–1643, 2021. 2, 6, 7
- [35] Chia-Wen Kuo, Chih-Yao Ma, Judy Hoffman, and Zsolt Kira. Structure-encoding auxiliary tasks for improved visual representation in vision-and-language navigation. In *WACV*, pages 1104–1113, 2023. 2
- [36] Joel Ye, Dhruv Batra, Erik Wijmans, and Abhishek Das. Auxiliary tasks speed up learning pointgoal navigation. *arXiv preprint arXiv:2007.04561*, 2020. 2
- [37] Chih-Yao Ma, Jiasen Lu, Zuxuan Wu, Ghassan AlRegib, Zsolt Kira, Richard Socher, and Caiming Xiong. Self-monitoring navigation agent via auxiliary progress estimation. In *ICLR*, 2019. 2, 7
- [38] Arjun Majumdar, Ayush Shrivastava, Stefan Lee, Peter Anderson, Devi Parikh, and Dhruv Batra. Improving vision-and-language navigation with image-text pairs from the web. In *ECCV*, pages 259–274. Springer, 2020. 3, 6
- [39] Aishwarya Agrawal, Jiasen Lu, Stanislaw Antol, Margaret Mitchell, C. Lawrence Zitnick, Dhruv Batra, and Devi Parikh. Vqa: Visual question answering. In *ICCV*, pages 2425–2433, 2015. 3
- [40] Hao Tan and Mohit Bansal. LXMERT: Learning cross-modality encoder representations from transformers. In *EMNLP*, pages 5103–5114, 2019. 3, 7
- [41] Vishnu Sashank Dorbala, Gunnar Sigurdsson, Robinson Piramuthu, Jesse Thomason, Gaurav S. Sukhatme. Clip-nav: Using clip for zero-shot vision-and-language navigation. In *CoRL*, 2022. 3
- [42] Alec Radford, Jong Wook Kim, Chris Hallacy, Aditya Ramesh, Gabriel Goh, Sandhini Agarwal, Girish Sastry, Amanda Askell, Pamela Mishkin, Jack Clark, et al. Learning transferable visual models from natural language supervision. In *ICML*, pages 8748–8763, 2021. 3
- [43] Jacob Devlin, Ming-Wei Chang, Kenton Lee, and Kristina Toutanova. BERT: Pre-training of deep bidirectional transformers for language understanding. In *NAACL*, pages 4171–4186, 2019. 6, 11
- [44] Xiangru Lin, Guanbin Li, and Yizhou Yu. Scene intuitive agent for remote embodied visual grounding. In *CVPR*, pages 7036–7045, 2021. 6
- [45] Angel Chang, Angela Dai, Thomas Funkhouser, Maciej Halber, Matthias Niebner, Manolis Savva, Shuran Song, Andy Zeng, and Yinda Zhang. Matterport3d: Learning from rgb-d data in indoor environments. In *3DV*, pages 667–676. IEEE, 2017. 6
- [46] Alexey Dosovitskiy, Lucas Beyer, Alexander Kolesnikov, Dirk Weissenborn, Xiaohua Zhai, Thomas Unterthiner, Mostafa Dehghani, Matthias Minderer, Georg Heigold, Sylvain Gelly, et al. An image is worth  $16 \times 16$  words: Transformers for image recognition at scale. In *ICLR*, 2020. 7, 11
- [47] Federico Landi, Lorenzo Baraldi, Marcella Cornia, Massimiliano Corsini, and Rita Cucchiara. Perceive, transform, and act: Multi-modal attention networks for vision-and-language navigation. *arXiv preprint arXiv:1911.12377*, 2020. 7
- [48] Yuankai Qi, Zizheng Pan, Shengping Zhang, Anton van den Hengel, and Qi Wu. Object-and-action aware model for visual language navigation. In *ECCV*, 2020. 7

## Appendix

We provide additional details and analysis of the proposed method in the supplementary material. Sec A presents further details of our overall model, while Sec B provides qualitative examples.

### A. Model Details

#### A.1. Algorithm Details

Algorithm 1 outlines the process of constructing proximity knowledge for regions. The construction of proximity knowledge for objects follows a similar procedure, with the only difference being that object proximity considers whether two objects are within a predefined spatial range. Figure 5 illustrates the images of our elaborately designed normalization function Eq. (1) and the proximity score adaptive function Eq. (14).

---

#### Algorithm 1: Constructing Region Proximity Knowledge

---

```

scans = nodes for each navigation scene
Initialize count_matrix
for nodes_list in scans do
    region_dict = classify_region(nodes_list)
    for sub_region in region_dict do
        for node in sub_region do
            cands=get_candidate_nodes_list(node)
            other_regions=get_other_regions(sub_region)
            if cands in other_regions then
                Update count_matrix
            end if
        end for
    end for
end for
proximity_pro=normalization_function(count_matrix)

```

---

#### A.2. Pretraining Details

In addition to the proposed Scene Understanding Auxiliary Task (SUAT), the model also utilizes four other

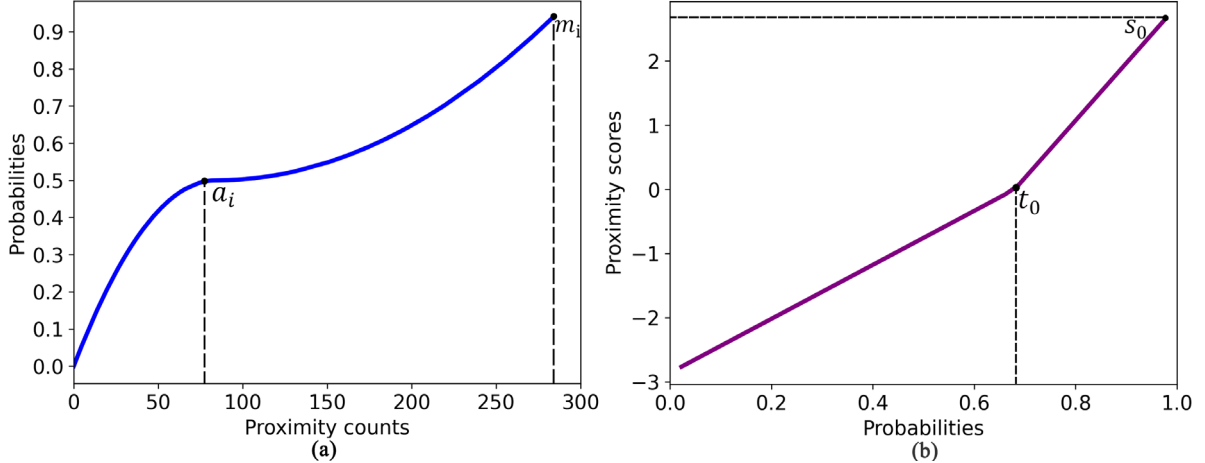


Figure 5. (a) Normalization function for transforming the proximity count matrix; (b) Proximity score adaptive function in PAAM.

auxiliary tasks for pretraining. In Sec 3.5, we have already introduced the Single-Step Action Prediction (SAP) and Object Grounding (OG) tasks. Here, we will provide a detailed explanation of the Masked Language Modeling (MLM) and Masked Region Classification (MRC) tasks.

**Masked Language Modeling (MLM).** The objective of MLM is to predict intentionally masked portions of text by leveraging the remaining contextual information, thereby fostering the model’s language understanding capabilities. This task takes language instructions  $\mathcal{W}$  and corresponding demonstration paths  $P$  as inputs. We incorporate the action scores predicted by DUET [11] in our approach, requiring the averaging of embeddings from both fine-grained and coarse-grained encoders. Subsequently, we employ a network consisting of two fully connected layers to predict the target word. We randomly mask 15% of the instruction tokens [43]. The task is optimized by minimizing the negative log-likelihood of the original words, denoted as  $L_{MLM} = -\log(w_i | L_m, P)$ , where  $L_m$  represents the masked instruction and  $w_i$  is the label of the masked token.

**Masked Region Classification (MRC).** The MRC task requires the model to predict semantic labels of masked view images based on the instruction, unmasked view images, and corresponding features in the semantic topological maps. We adopt a setting almost identical to DUET, where in the fine-grained encoder, we randomly mask the last observed visual image and object corresponding to the demonstration path  $P$  with a probability of 15%. The only difference is that we incorporate the features of region-view images and their contained objects as inputs. The visual features of the masked images or objects are set to zero while preserving their positional embeddings. The target semantic labels for view images are predicted by a pretrained image classification model [46] on ImageNet, while the object labels are obtained from a pretrained object detector [4] on the Visual Genome dataset [16]. Similar to MLM, we

employ a two-layer fully connected network to predict the semantic labels of the masked visual tokens and minimize the KL divergence between the predicted and target probability distributions.

## B. More Qualitative Results

### B.1. Multi-scale Spatial Proximity Knowledge

Figure 6 presents the visualized results of the region proximity knowledge constructed through the auxiliary task. It can be observed that there are many spatial proximity probabilities between different regions that are zero, while some exhibit a probability of one. Our proposed method ensures the accuracy of these probabilities, whereas the extracted spatial proximity probabilities from the knowledge base tend to an average value, there is no such absolute yet precise spatial proximity probabilities. In other regions, the region proximity knowledge constructed by our model also conforms to common sense. For example, dining rooms are generally adjacent to kitchens, bedrooms are adjacent to bathrooms, and hallways are adjacent to stairs.

Table 8 presents a partial display of the region-object proximity knowledge constructed from the auxiliary tasks. It can be observed that objects such as beds and wardrobes are associated with bedrooms, while objects like sofas and

Region	Top 5 relevant objects
bedroom	bed, desk, pillow, lamp, wardrobe,
dining room	table, chair, chandelier, cup, microwave
living room	couch, table, television, bookshelf, armchair
office	desk, chair, laptop, mouse, printer
gym	treadmill, dumbbells, bench, ball, fire extinguisher

Table 8. Proximity knowledge of region-object constructed from auxiliary tasks.

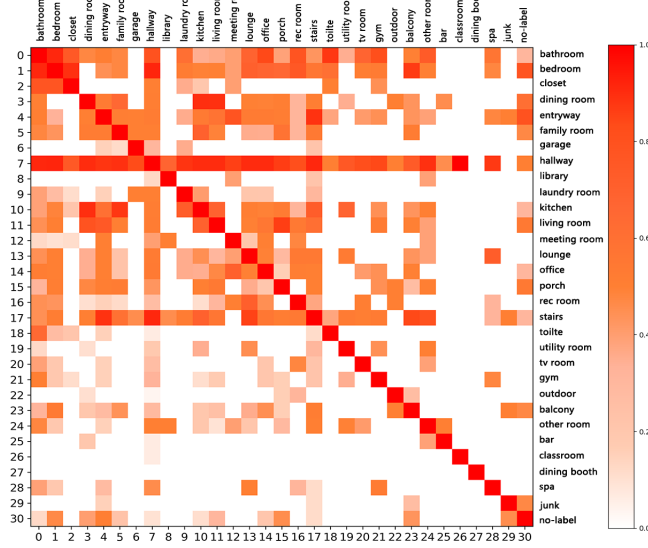


Figure 6. Proximity knowledge of regions constructed from auxiliary tasks.

televisions are associated with living rooms, which aligns well with the real-world indoor environment. These findings also demonstrate the validity and reliability of our designed SUAT.

## B.2. Qualitative Examples

Figure 7 visualizes the reasoning navigation process of our HSPR in the REVERIE [2] unseen environment and compares it with the baseline. The figure displays panoramic views and the inferred paths for each step. At step 1, the HSPR agent finds three navigable nodes belonging to different regions, namely the hallway, dining room, and living room. Through the Multi-step Reasoning Navigation Algorithm (MRNA), the agent plans the optimal path. At step 2, a navigable node belonging to a new region, the office, is discovered, and the proximity between the office and the sub-target, the bathroom, is found to be 0.83, so the agent re-plans the optimal path. Then the agent finally reaches the target area in the process of constantly planning and searching for sub-target. Utilizing the object proximity knowledge, the agent accurately predicts the bounding box of curtain, based on the window at step 6. In contrast, the DUET [11] agent completely deviates from the shortest path at step 5 and then explores the environment continuously to find the target region, ultimately reaching the maximum navigation steps and being forced to terminate. Although the DUET agent identifies the curtain, it stops at the wrong position, indicating the need for additional knowledge-based guidance during the navigation process instead of near-blind exploration.

Figure 8 visualizes a long trajectory navigation example where the DUET model fails, while our HSPR model

succeeds. At step 1, the agent infers the optimal path based on the current navigable nodes. At steps 2 and 5, it discovers navigable nodes belonging to new regions and re-plans the path accordingly. At step 6, when the sub-target is not found, the agent selects a sub-optimal path and backtracks to the navigable node with the highest action scores, finally reaching the target region along the inferred path. The target of this navigation is to find clothes in the washing machine, so we utilize the object proximity knowledge to better localise the objects through the space where the washing machine and laundry detergent are localised.

Figure 9 showcases a navigation failure example of the HSPR model, indicating that even if the agent is on the correct path to the target, it may not be able to stop at the target. Specifically, at step 3, the agent self-assumes to have arrived at the target region, but with a relatively low stop action score, it decides to continue exploring and backtrack. At step 6, the agent arrives at the actual target region but seems unable to identify the pot. Throughout steps 7 to 10, the agent continuously roams within the target region without successfully identifying the target object. At step 11, the agent decides to backtrack to step 3, which mistakenly identified the dining room as the family room, ultimately localising the pot on the table and causing the navigation task to fail. This signifies the need for further improvement in our model’s image encoder to enhance the encoding of visual representations of scenes, thereby improving scene recognition and fine-grained object grounding capabilities.

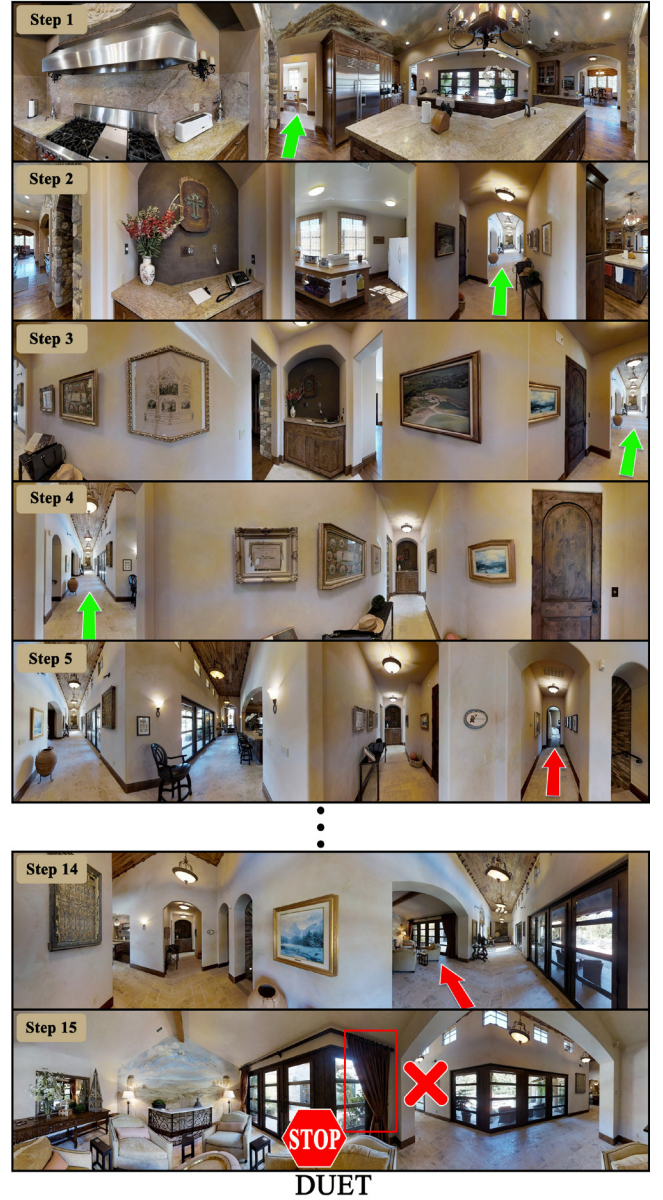


Figure 7. Navigation examples of HSPR and DUET [11] model. The left side shows our HSPR model, while the right side represents the baseline DUET model. HSPR model utilizes proximity knowledge constructed from the auxiliary tasks for reasoning navigation to complete the navigation task along the shortest path. In contrast, the DUET model reaches the maximum navigation steps during continuous exploration and stops in the wrong region.

Instruction: “Please go to the laundry room and load the washing machine on the left side.”



Figure 8. Example of successful HSPR model navigation. The agent continuously plans the optimal path to the target region by using the MRNA from step 1 to 5. At step 6, it is found that the sub-target cannot be found, and the sub-optimal path is selected and backtracked. After that, we reach the target region along the reasoning path, and use the object proximity knowledge to assist the target object grounding.

Instruction: “Head to the family room on level 2 and put away the pot.”

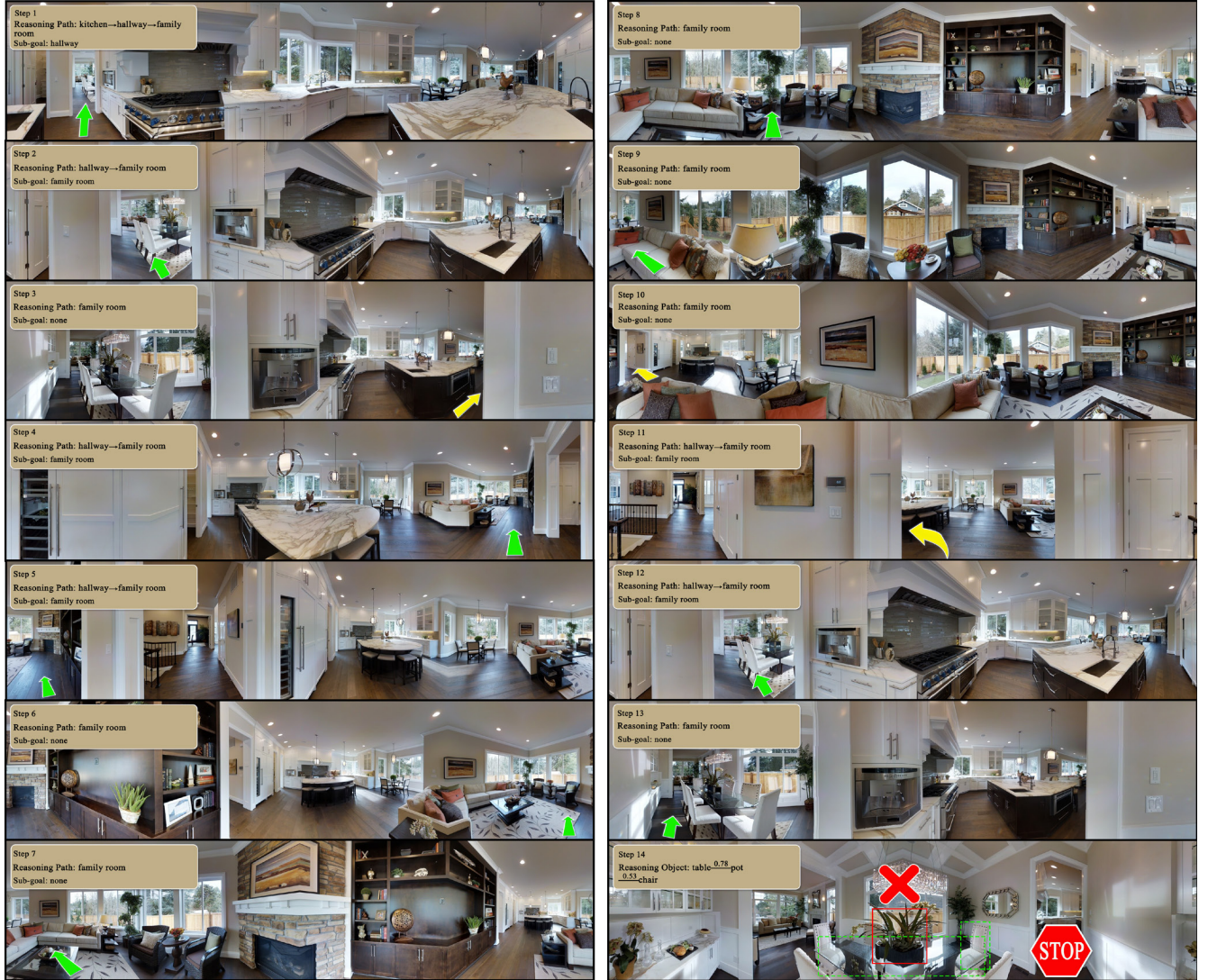


Figure 9. Example of navigation failure in the HSPR model. At step 3, the agent identifies the dining room as the target region but does not decide to stop there, opting instead to continue exploring other regions. Despite reaching the actual target region starting from step 6, the agent consistently fails to localise the target object. At step 11, it backtracks to the location of step 3 and eventually localises the pot on the table.